Energy Materials

Supplementary Materials

Advancing kesterite absorbers with bronze-based precursors through physical deposition routes: a step toward stable and sustainable industrial photovoltaic technology

Robert Fonoll-Rubio[1], Jesús Roberto González-Castillo[2], Jacob Andrade-Arvizu[1], Xavier Alcobé[3], Alejandro Pérez-Rodríguez[1,4], Pedro Vidal-Fuentes[1], Maxim Guc[1,*], Victor Izquierdo-Roca[1,*]

[1]Catalonia Institute for Energy Research (IREC), Sant Adrià de Besòs-Barcelona 08930, Spain.
[2]Escuela Superior de Física y Matemáticas - Instituto Politécnico Nacional (ESFM - IPN), Ciudad de México 07738, México.
[3]Centres Científics i Tecnològics (CCiTUB) de la Universitat de Barcelona, Barcelona 08028, Spain.
[4]Departament d'Enginyeria Electrònica i Biomèdica, IN2UB, Universitat de Barcelona, Barcelona 08028, Spain.

[*]**Correspondence to:** Dr. Victor Izquierdo-Roca, Catalonia Institute for Energy Research (IREC), Jardins de les Dones de Negre 1, Sant Adrià de Besòs-Barcelona 08930, Spain. E-mail: vizquierdo@irec.cat; Dr. Maxim Guc, Catalonia Institute for Energy Research (IREC), Jardins de les Dones de Negre 1, Sant Adrià de Besòs-Barcelona 08930, Spain. E-mail: mguc@irec.cat

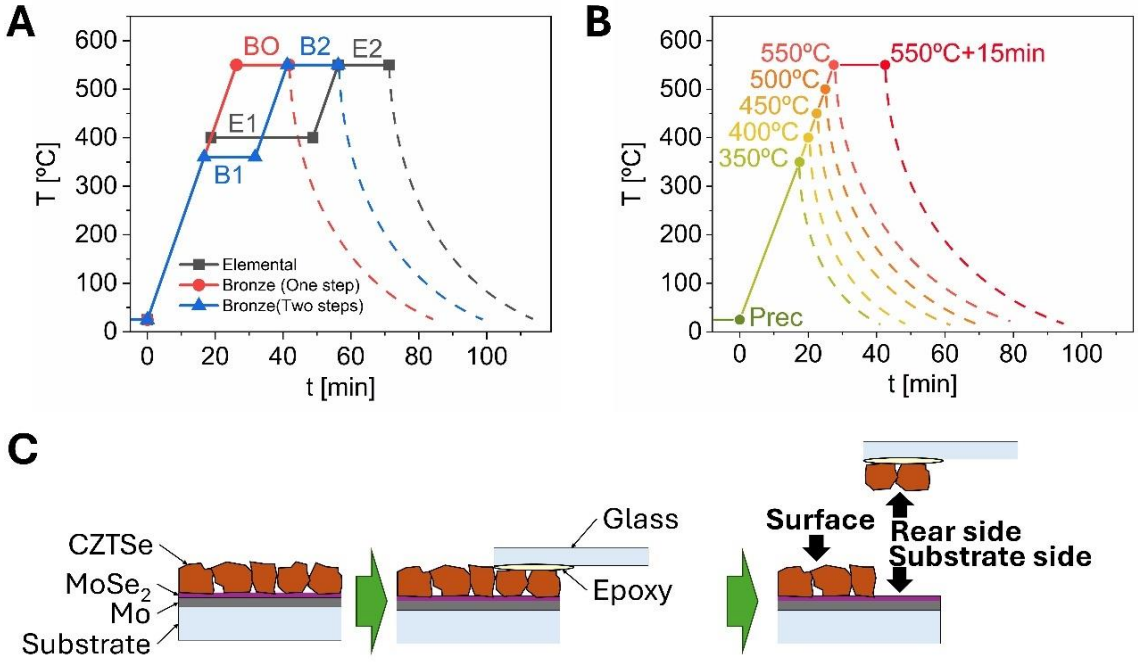

Supplementary Figure 1. (a) Evolution of the annealing process temperature as a function of the time for the comparative study of the elemental and bronze-based precursors. For the bronze-based precursor, a one-step and a two-step annealing processes were applied. For the elemental precursor, only the two-step annealing process was applied. The synthesis conditions of the different steps are: (E1) 400 °C, 30 min, 1.5 mbar (Ar pressure); (E2) 550 °C, 15 min, 1 bar; (BO) 550 °C, 15 min, 400 mbar; (B1) 360 °C, 15 min, 400 mbar; (B2) 550 °C, 15 min, 900 mbar. (b) Evolution of the annealing temperature as a function of the time for the study of the impact of the germanium doping on bronze-based precursors. A one-step annealing processes was applied to Ge-free and Ge-doped bronze-based precursors consisting in a 20 °C/min heating ramp, and samples were processed at 350 °C, 400 °C, 450 °C, 500 °C, and 550 °C, and at 550 °C with a 15 min dwell at this temperature. In all cases, the absorbers were naturally cooled to room temperature after the annealing process. In addition, all precursors were individually placed into a 3.8 cm^3 graphite box with 100 mg of Se and 5 mg of Sn in the case of the elemental precursor, and with 200 mg of Se and 5 mg of Sn in the case of the bronze-based precursor. (c) Schematic representation of the mechanical lift-off process consisting in attaching a region of the absorber surface to a glass by means of an epoxy adhesive and, afterwards, pulling that glass and the substrate in opposite directions to detach a portion of the absorber from the substrate.

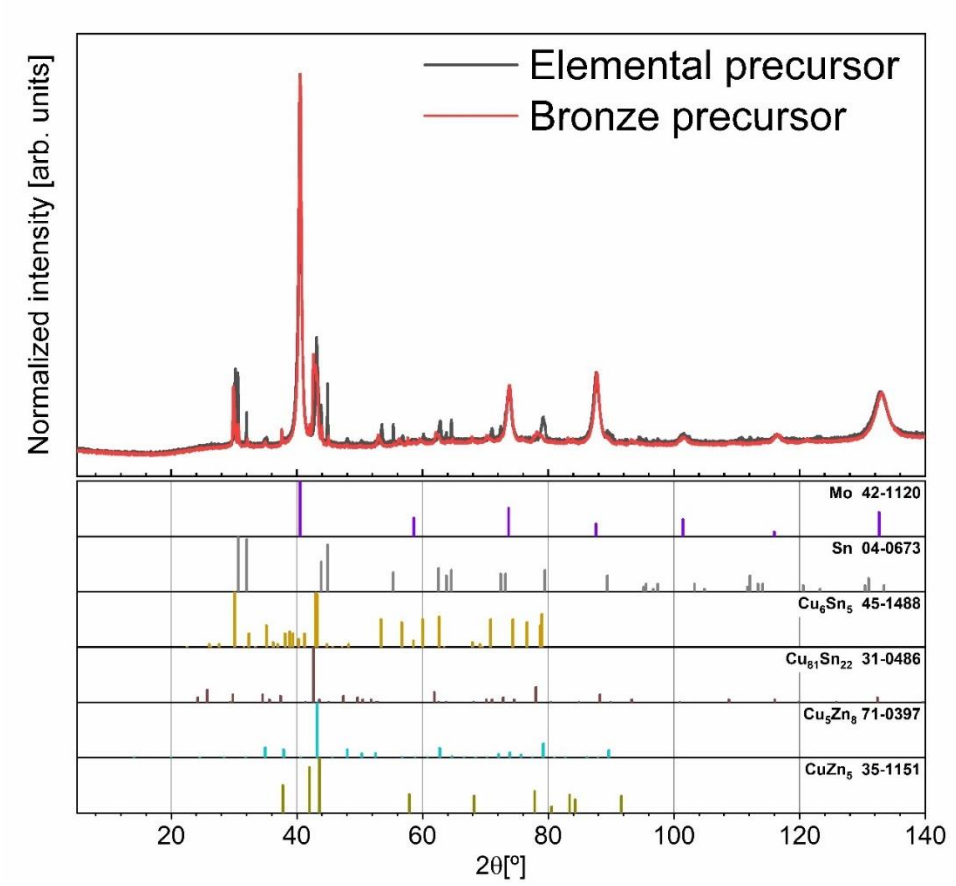

Supplementary Figure 2. XRD pattern of the elemental metallic stack precursor and the bronze-based precursor. Patterns are normalized to Mo reflections at 40.5°.

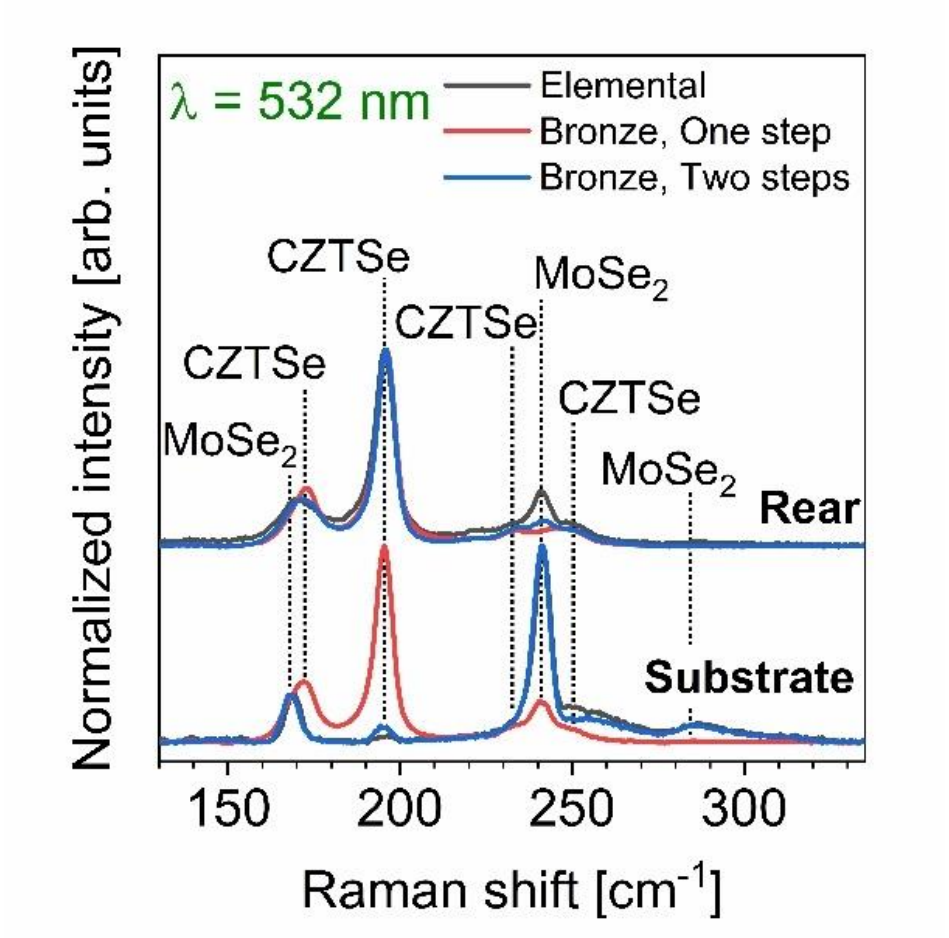

Supplementary Figure 3. Macro-Raman spectra measured under 532 nm excitation at the rear interface of CZTSe absorbers synthesized from an elemental metallic stack precursor and from bronze-based precursors. In the second case, different absorbers were synthesized by applying a one-step and a two-step annealing processes. The measurements were performed after mechanical lift-off of the absorber layer and measuring both the exposed rear side of the absorber and the exposed substrate side (see **Supplementary Figure 1C**). These results reveal that the detachment of the absorber was produced by the CZTSe/$MoSe_2$ interface in the case of the two-step annealing process for both types of precursors, as indicated by the predominant detection of CZTSe at the exposed rear side of the absorber and the predominant detection of $MoSe_2$ at the exposed substrate side. However, in the case of the one-step annealing process, the separation was produced by an interface between big and small CZTSe grains, as indicated by the predominant detection of CZTSe at both exposed sides and considering the bilayer structure observed by SEM in **Figure 3**.

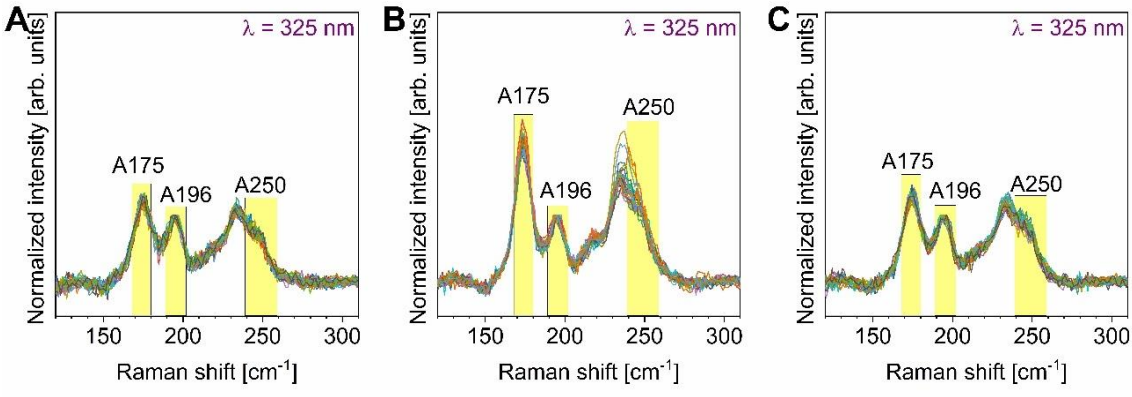

Supplementary Figure 4. Macro-Raman spectra measured under 325 nm excitation on CZTSe absorbers synthesized from (a) an elemental metallic stack precursor, (b) a bronze-based precursor and a one-step annealing process, and (c) a bronze-based precursor and a two-step annealing process. Integrated areas are highlighted in the spectra.

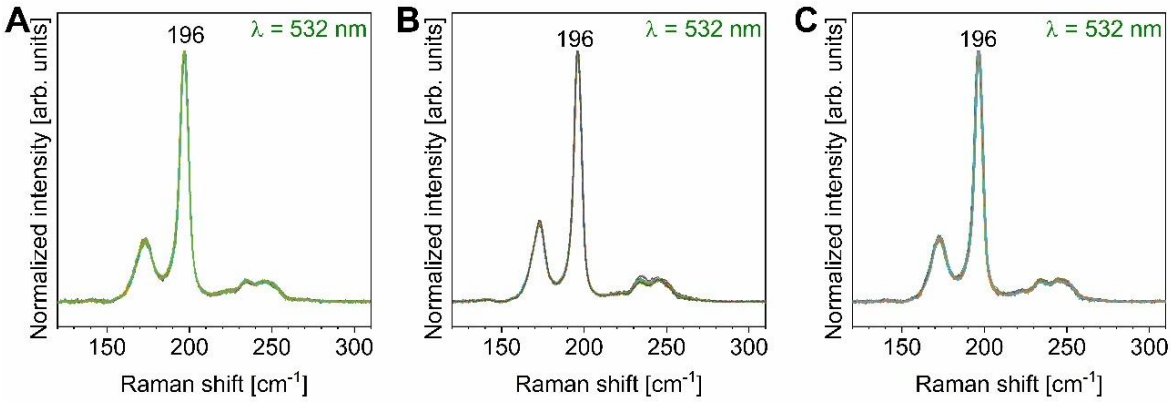

Supplementary Figure 5. Macro-Raman spectra measured under 532 nm excitation on CZTSe absorbers synthesized from (a) an elemental metallic stack precursor, (b) a bronze-based precursor and a one-step annealing process, and (c) a bronze-based precursor and a two-step annealing process. Peak at 196 cm^{-1} is indicated in the spectra.

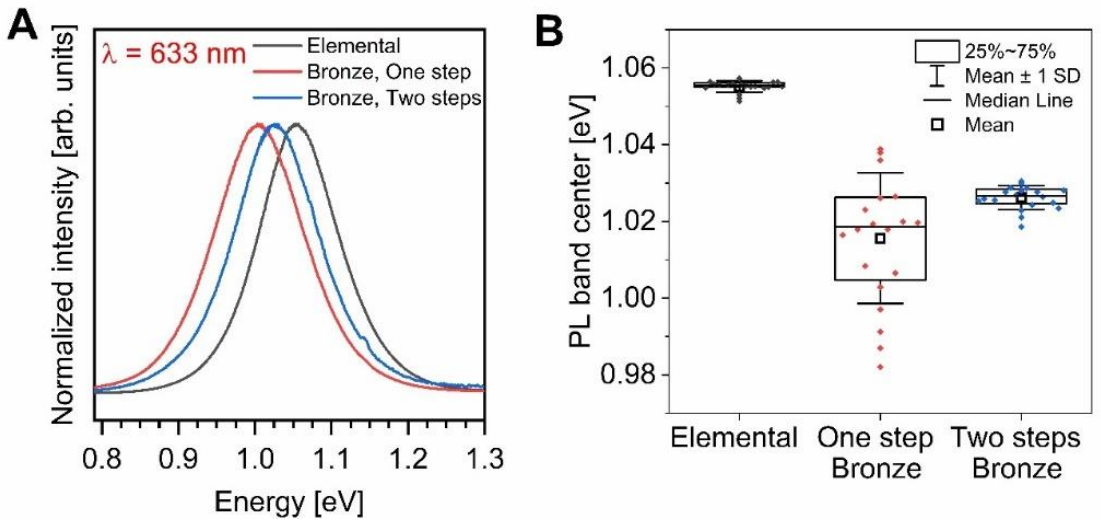

Supplementary Figure 6. (a) Average photoluminescent spectra of CZTSe absorbers obtained from an elemental metallic stack precursor and from bronze-based precursors. (b) Center of the PL band obtained by Gaussian fit of the PL spectra measured in different points of the previous CZTSe absorbers.

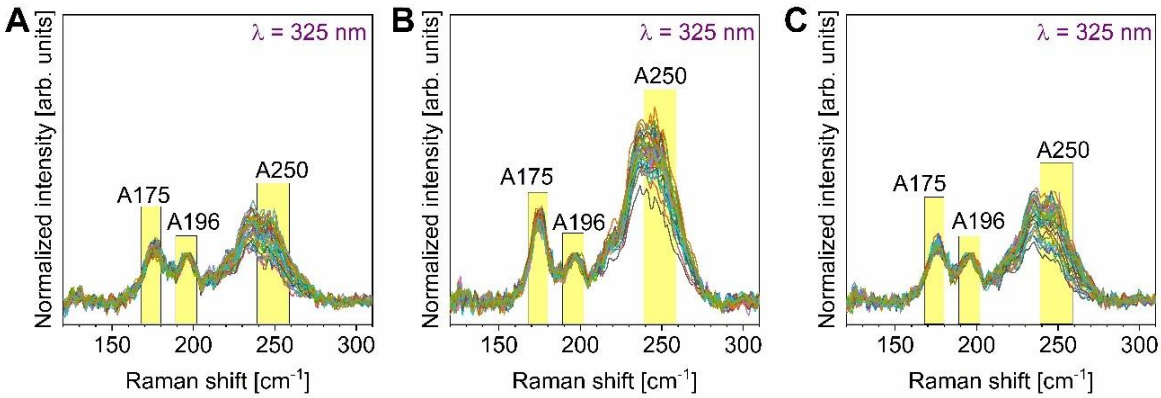

Supplementary Figure 7. Micro-Raman spectra measured under 325 nm excitation on a 50 x 50 μm^2 area of CZTSe absorbers synthesized from (a) an elemental metallic stack precursor, (b) a bronze-based precursor and a one-step annealing process, and (c) a bronze-based precursor and a two-step annealing process. Integrated areas are highlighted in the spectra.

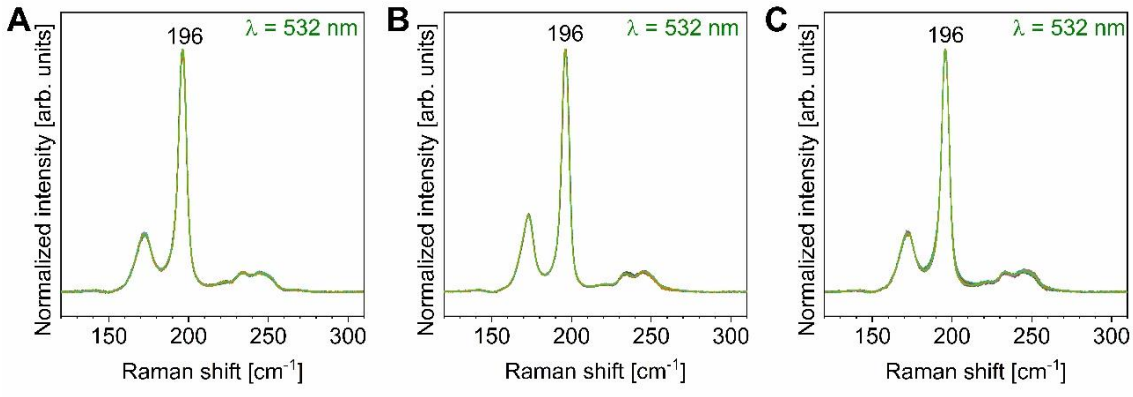

Supplementary Figure 8. Micro-Raman spectra measured under 532 nm excitation on a 50 x 50 μm^2 area of CZTSe absorbers synthesized from (a) an elemental metallic stack precursor, (b) a bronze-based precursor and a one-step annealing process, and (c) a bronze-based precursor and a two-step annealing process. Peak at 196 cm^{-1} is indicated in the spectra.

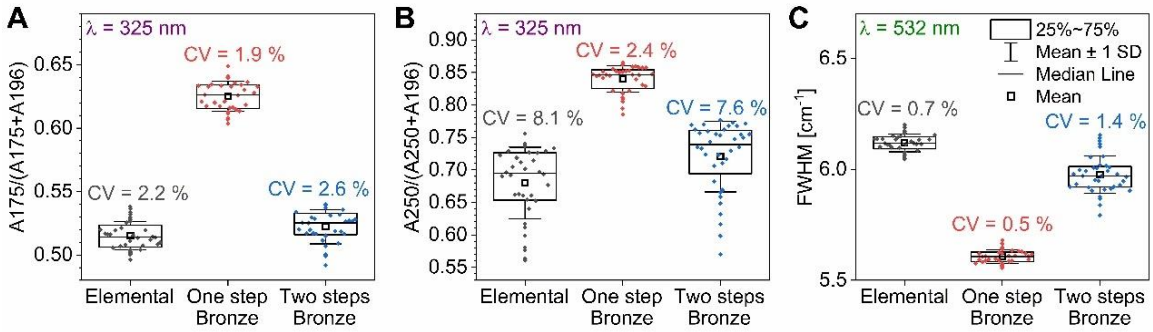

Supplementary Figure 9. (a) Relative integrated intensity of the 175 cm^{-1} peak, (b) relative integrated intensity of the 250 cm^{-1} peak, and (c) full width at half-maximum of the 196 cm^{-1} peak obtained by micro-Raman spectroscopy under 325 and 532 nm excitation on a 50 x 50 μm^2 area of CZTSe absorbers synthesized from an elemental metallic stack precursor and from bronze-based precursors. In the second case, different absorbers were synthesized by applying a one-step and a two-step annealing processes. The coefficient of variation is indicated for each parameter and sample.

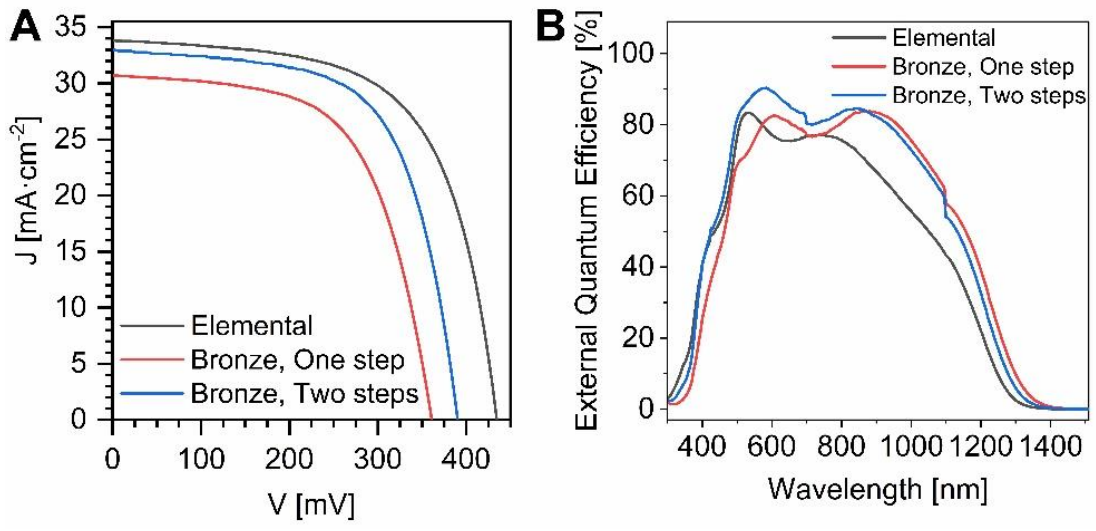

Supplementary Figure 10. (a) Current density-voltage curves of the CZTSe-based solar cells with the highest energy conversion efficiency obtained from an elemental metallic stack precursor and from bronze-based precursors. (b) EQE curves of the CZTSe-based solar cells with the highest integrated EQE obtained from the previous precursors. In the bonze-based case, different devices were produced by applying a one-step and a two-step annealing processes.

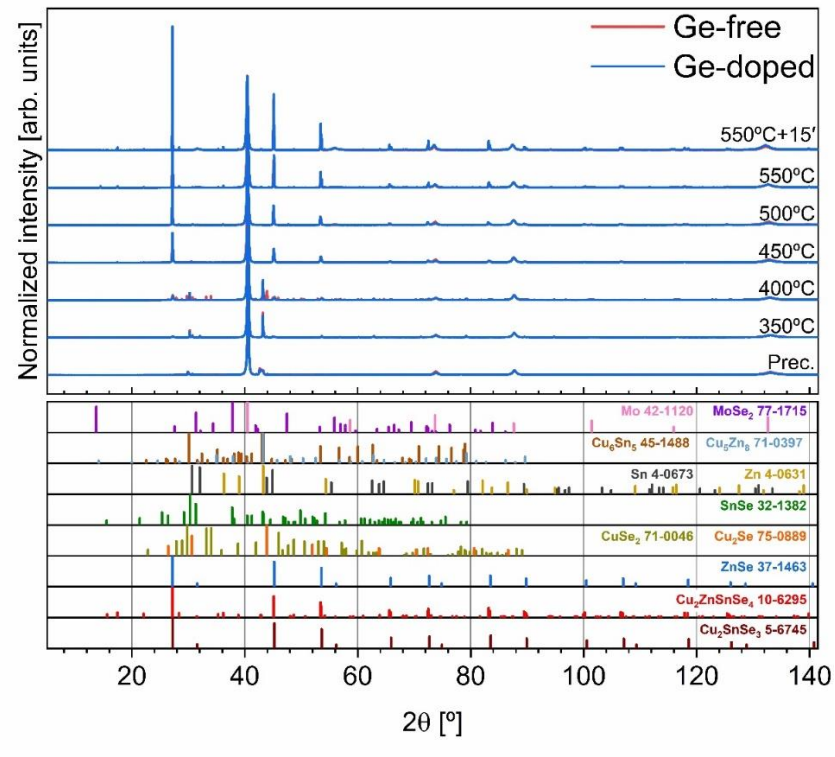

Supplementary Figure 11. XRD patterns of samples produced at different stages of a one-step annealing process from Ge-free and Ge-doped bronze-based precursors.

Patterns are normalized to Mo reflection peak at 40.5°. Under the measured diffractograms, the patterns of different phases observed during the formation are listed and the numbers behind each phase correspond to reference patterns in ICDD database.